Computer Standards & Interfaces 58 (2018) 109–117

Contents lists available at ScienceDirect

Computer Standards & Interfaces

journal homepage: www.elsevier.com/locate/csi

Analyzing lifetime of energy harvesting wireless multimedia sensor nodes in industrial environments

Nazli Tekin, H. Emre Erdem, V. Cagri Gungor*

Department of Computer Engineering, AGU, Kayseri, Turkey

ARTICLE INFO

Keywords:
Energy harvesting
Image compression
Lifetime
Wireless sensor networks

ABSTRACT

Recently, there has been a great demand for multimedia communication using Wireless Multimedia Sensor Networks (WMSNs) in industrial environments thanks to their low cost, flexibility, and rapid deployment. However, WMSNs face a major challenge of limited lifetime due to their limited battery capacity. Compared to regular data transmission, multimedia data transmission causes higher energy consumption because of larger data sizes leading to faster depletion of sensor node's batteries. The objective of this paper is to analytically quantify the impact of different energy harvesting methods based on vibration, indoor solar, and temperature difference as well as Fast-Zonal DCT and BinDCT based image compression methods on the lifetime of Telos and Mica2 sensor nodes deployed in indoor industrial environment. Performance results show that energy harvesting and image compression techniques improve lifetime of Mica2 and Telos motes by 51.8% and 25.8%, respectively when used with proper power management methods.

1. Introduction

Recently, Wireless Multimedia Sensor Networks (WMSNs) have gained great interest thanks to their low cost and collaborative intelligence. The applications of WMSNs span a very wide range, including surveillance monitoring, traffic monitoring, personal health care, smart farms, agricultural monitoring, and industrial monitoring systems. In surveillance applications, multimedia sensors can be used to detect enemy intrusions, monitor public areas, private properties or borders and prevent malicious activities. For instance, surveillance systems are used to check for suspicious behaviors in smart city applications [1]. In traffic monitoring applications, it is possible to identify the presence of a violator by monitoring roads and highways. Also, WMSNs are used in smart parking advisory systems for monitoring available parking lots. In personal health care applications, patients can be remotely monitored by means of audio or video sensors [2]. In smart farm and agriculture applications, animals' situation and crop status can be remotely monitored for condition analysis [3]. Moreover, WMSNs can be used in industrial facilities to observe the status of machineries and materials via the acquisition of real-time data [4]. For instance, manufacturers prefer live monitoring of tool and machineries used in factory environments for the prevention of possible failures that may result in high repair costs or temporary cessation of operations [5]. Therefore, WMSNs can deliver flexibility to computer vision based visual analysis and automated activities which require fast and intermittent operation [6]. In various industrial applications, multimedia sensors are used to ensure the quality of new products to check whether they match the defined standards. Additionally, these sensors are used in control of industrial robots [7]. In addition, information on surroundings in a dynamic environment through which an industrial mobile robot is traveling may be provided by sensors that are distributed across the environment. Finally, sensor networks may help to enforce the environmental regulations that require industries to follow local and federal laws governing the protection of the environment [4].

WMSNs are composed of multiple sensor nodes which possess CPU, radio and battery components as well as various sensor modules, such as cameras. These sensor nodes have three main capabilities, which are sensing to collect data from the environment, processing to analyze the gathered data and transmitting to relay data to other sensor nodes or a sink node [8]. However, sensor nodes present the disadvantage of having limited energy due to their built-in battery, narrow bandwidth due to channel conditions and reduced memory due to energy costs [9]. The acquisition and transmission of multimedia data pose additional challenges for WMSNs. Larger size of multimedia data provokes higher processing and transmission costs. These problems may pose significant risks in industrial applications, since the monitored assets may have critical role on production. For example, temporary interruption of a restricted area monitoring system due to battery depletion may cause

* Corresponding author.
E-mail addresses: nazli.tekin@agu.edu.tr (N. Tekin), huseyin.erdem@agu.edu.tr (H.E. Erdem), cagri.gungor@agu.edu.tr (V.C. Gungor).

https://doi.org/10.1016/j.csi.2017.12.005
Received 21 April 2017; Received in revised form 11 December 2017; Accepted 17 December 2017
Available online 18 December 2017
0920-5489/

critical problems. Therefore, maximizing lifetime of sensor nodes plays a vital role especially in WMSN applications.

In WMSNs, lifetime improvement can be achieved by decreasing energy consumption utilizing better power management methods and adopting data size reduction methods. In addition, energy harvesting may help prolong lifetime by increasing available energy amount.

To conserve energy, several power management methods have been proposed in the literature. For instance, a method called schedule-driven model, which aims to alternate sensor nodes between active and sleep mode based on predetermined duty cycle and duty period is proposed. The schedule-driven operation is constructed using a semi-Markov chain to model the inter-mode transitions of sensor node [10].

In addition to power management methods, data size reduction methods are essential for energy conservation since computation requires less energy than transmission [11]. Multimedia contents, especially real-time video streams, require high bandwidth and higher data rate than supported commercial sensors [2]. Thus, this paper focuses on low data rate industrial multimedia applications (i.e. image transmission), such as monitoring and tracking of machinery, with the main purpose of decreasing the energy consumption and maximizing sensor node's lifetime. Therefore, to reduce the data size and save the battery power, the sensor node exploits image compression methods. However, compressing multimedia data may not provide energy conservation over the transmission of the same data without compression based on the compression method used [12]. In other words, the compression process may be very costly in terms of CPU processing power. Hence, the computation cost of data compression must be taken into consideration. Most compression methods are based on Discrete Cosine Transformation (DCT). However, the energy consumption of DCT is also high because of the intensive computations required. BinDCT is fast multiplierless approximations of DCT. For this reason, Fast-Zonal BinDCT approach that diminishes the computation cost is preferred [13].

Utilizing energy harvesting devices to support batteries of industrial sensor nodes is considered another promising opportunity for the efficiency and sustainability of WMSN-based industrial applications. In this respect, energy harvesting can be performed exploiting various resources, such as solar, thermal, electromagnetic, and mechanical energy [14]. However, the above-mentioned resources are not abundant in indoor industrial environments. In this paper, our goal is to analyze the lifetime of a wireless multimedia sensor node transmitting image data when various types of harvesters are used in industrial environments. In summary, the main contributions of this paper are as follows:

- The impact of indoor solar harvesting, thermal harvesting, and vibration harvesting on sensor node lifetime is analyzed,
- To what extent compressing the image before transmitting affects the lifetime is investigated,
- In contrast to previous works, realistic wireless channel model to better represent the channel conditions of an industrial environment is utilized,
- How different duty cycle requirements of applications affect node's lifetime using schedule-driven power management scheme is examined.

The remainder of this paper is organized as follows. Section 2 discusses the work previously conducted on sensor node lifetime, image compression techniques, and energy harvesting methods. Section 3 presents methods practiced in this study. Section 4 demonstrates the performance results. Finally, Section 5 concludes the paper.

2. Related work

Compared to regular Wireless Sensor Network (WSN) applications, nodes in image based WMSN applications consume more energy while transmitting image data due to larger size of data to be sent. In literature, image compression algorithms have been developed in order to reduce the number of bits to send. For instance, Nasri et al. [15] described the advantage of using JPEG2000 image compression method in WSNs. They proposed a distributed image compression scheme in which nodes compress data before forwarding. It is shown that this proposed scheme improves network lifetime.

Huu et al. [16] proposed an algorithm which allocates energy cost for image compression among the nodes by distributing image compression workload among clusters in WSNs. Energy threshold adaptation algorithm is applied to control residual energy of sensor nodes in WSN. In this algorithm, relay node and dynamic threshold value are determined according to sensor nodes' remaining energy. The proposed algorithm provides balanced energy consumption among sensor nodes and increases network lifetime.

Sun et al. introduced the Low Energy Image Compression Algorithm (LEICA) [17]. LEICA divides images into regions to separate background from point of interest. This method compresses the least significant part of an image such as background using high compression ratio whereas the interested part of the image using low compression ratio. Therefore, the method consumes less energy in image compression.

Li et al. proposed a modified compression algorithm [18]. They combined the SPHIT compression algorithm with Huffman encoding. This method significantly reduces the number of bits to send in image transmission.

Wei et al. designed a Distributed Multi-node Cooperative Network (DMCN) to enhance the energy consumption of the network [19]. They proposed a Noise-tolerant Distributed Image Compression algorithm based on Principal Component Analysis (NDIC-PCA) for image compression. In this compression method, the sensor node partitions the image and forwards it to the cluster head which compresses these partitioned images. Therefore, this method provides high image quality with high compression ratio.

To reduce energy consumption involved in image transmission Hemalatha et al. [20] proposed Compressed Sensing (CS) based image transmission. The proposed block by block basis encoding algorithm allows capturing and representing compressible signals in relatively low measurements. Therefore, it is shown that energy consumption for the image compression is substantially reduced.

Nikolakopoulos, George, et al. [21] have proposed a novel transmission scheme which uses quad tree decomposition algorithm and fast image inpainting algorithm for compression and restoration of the images, respectively. By combining these two algorithms, they achieved both good quality transmitted images and relatively reduced cost of compression.

Kidwai et al. [22] have introduced a Zero-Memory Set Partitioned Embedded bloCK (ZM-SPECK) coder which is a fast and memoryless image coder. This coder calculates Discrete Wavelet Transform (DWT) coefficients by using fractional wavelet filter. With this algorithm, they reduced the memory required in transform and coding stage. Moreover, this algorithm reduced the computational complexity.

Orhan et al. [23] have investigated source and channel coding for energy limited WSN nodes. They considered time slotted system to model the fluctuations on the source and channel over time. They aim to diminish the distortion between source and reconstructed samples by finding optimal compression and transmission policies.

Calvo-Fullana et al. [24] have investigated reconstructing time-correlated data in a point-to-point topography with an energy-harvesting sensor and a Fusion Center (FC). Their aim is to reconstruct the data with less degradation exploiting previously encoded data. They have defined the problems in convex optimization framework. To solve the problems, they have proposed a procedure which uses the subgradient method iteratively.

In addition to compression methods, energy harvesting systems also provide a solution for limited lifetime. Energy harvesting sources can be categorized into two categories which are ambient sources and external sources [14]. One example for ambient source usage is Radio Frequency (RF) based energy harvesting system. RF-based energy harvesting system converts the energy of RF signal into electrical energy. Shigeta et al.

presented software control method to maximize sensing rate of WSNs by using RF ambient power in their study [25].

Solar energy is another example of ambient sources. Despite the lower amounts of light compared to direct sunlight, artificial lightning systems used in industrial environments may still enable indoor solar based energy harvesting with lower power output. For instance, Hande et al. developed a method for energy harvesting exploiting fluorescent lights to power sensor nodes in indoor environments [26].

Additionally, thermal energy is also considered as an ambient energy source. Thermal energy harvesters transform thermal energy (heat) into electrical energy by using the Seebeck effect. Elefsiniotis et al. investigated the performance of thermal harvesting devices with a Thermo Electric Generator (TEG) powering wireless sensors for aircraft applications [27].

On the other hand, the mechanical energy to be used in energy harvesting system is classified as an external source. The mechanical energy vibrations, pressure, and strain possess can be transformed into electrical energy via electromagnetic, electrostatic or piezoelectric mechanisms. Karimi et al. examined the amount of energy harvested from bridge vibrations using a piezoelectric energy harvester [28]. In industrial applications, using piezoelectric materials to harvest vibration energy from motor or machine vibrations is of great interest. However, time varying nature of the vibrations in such environments remains a challenge. Sankman and Dongsheng [29] have proposed an adaptive impedance matching piezoelectric energy harvesting system for time varying vibrations to increase the efficiency of harvester.

All these existing studies provide valuable insights on image compression techniques and energy harvesting methods. However, none of them presents a detailed evaluation of a sensor node lifetime combining both energy harvesting methods and compression techniques while considering industrial radio propagation characteristics and sensor node power management schemes.

3. Evaluated methods and protocols

This study focuses on industrial environments where communication channel show different characteristics and the environment propose unique conditions for energy harvesting. To better emulate the channel conditions, log normal shadowing channel model with parameters based on actual industrial environment measurements are used. Moreover, the availability of ambient resources for energy harvesting are also based on actual measurements. More detailed explanations on these methods are provided in the following sections.

3.1. Channel model

In industrial environments, electromagnetic signal propagates but it may be scattered, reflected or diffracted. This is due to environmental factors, such as signal bouncing on walls or machines. Therefore, signal strength declines and is randomly and log normally distributed. Due to the fact that it provides a more accurate channel model [30], the log normal shadowing model is preferred in this paper. The path loss $PL(d)$ formula for this model is shown by:

$$PL(d) = PL(d_0) + 10n\log_{10}\left(\frac{d}{d_0}\right) + X_\sigma, \tag{1}$$

where d and d_0 represents the transmission distance and the reference distance, respectively. n denotes the path loss exponent, and X_σ indicates a Gaussian random variable (in dB) with zero mean and σ standard deviation. Also, $PL(d_0)$ symbolizes the path loss in dB.

Signal-to-noise ratio (SNR) γ at distance d is computed as follows:

$$\gamma(d) = P_t - PL(d) - P_n, \tag{2}$$

where P_t is the output power and P_n is the noise floor. O-QPSK is implemented as a modulation scheme in Telos motes and the Bit Error Rate (BER) is shown by (3) [31]:

$$P_b^{OQPSK} = Q(\sqrt{(E_b/N_o)_{DS}}), \tag{3}$$

where,

$$(E_b/N_o)_{DS} = \frac{(2N \times E_b/N_o)}{(N + 4E_b/N_o(K-1)/3)}. \tag{4}$$

In (4), K and N represents the number of users and the number of chips per bit, respectively. FSK is implemented as a modulation scheme in Mica2 motes and the Bit Error Rate (BER) is shown by (5) [32]

$$P_b^{FSK} = \frac{1}{2}e^{-\frac{E_b/N_o}{2}}, \tag{5}$$

where,

$$E_b/N_o = \psi\frac{B_N}{R}. \tag{6}$$

In (6), ψ is the received SNR, B_N is the noise bandwidth, and R is the data rate.

When the channel conditions in industrial environments are bad, the sensor node retransmits the data packet to provide reliable communication. However, all these retransmissions lead to higher energy consumption. Hence, for estimating the sensor node lifetime, the Packet Reception Rate (PRR), which denotes the ratio of successfully transmitted packets to the number of all packets should be calculated. Combining the bit error rates together with the corresponding encoding scheme NRZ [30], PRR can be calculated using:

$$PRR = (1 - P_b)^{8l}(1 - P_b)^{8(f-l)}, \tag{7}$$

where P_b represents BER, f is the frame size and l is the preamble.

3.2. Image compression methods

To decrease energy consumption of wireless sensor nodes while transmitting image, compression methods have been proposed. Data size is a crucial factor during transmission in terms of energy requirements of the sensor node. Although data size reduction may help to decrease energy consumption in the transmission stage, it may cause higher energy consumption in the computation stage. Therefore, the computation cost of compression should be taken into account.

3.2.1. Fast zonal DCT based image compression

Discrete Cosine Transformation (DCT) is applied to most image compression schemes since it delivers optical decorrelation efficiency [33]. DCT is a technique which transforms image from spatial domain into frequency domain hereby removes spatial redundancy of an image and extract powerful values of an image [34]. In DCT algorithm, image is divided into 8×8 blocks of pixels. Later DCT is applied to each block to compress starting from top left part of image. A compressed image is constituted after quantized and encoded.

DCT algorithm is highly demanding in terms of computation power [35]. To reduce the computation cost, zonal coding approach is preferred in this study. In zonal coding, only the coefficients for the selected sub-region among 64 DCT coefficients are computed and encoded. The selected sub-region which is specified by parameter k is defined using either a square pattern or a triangle pattern. In square pattern, only upper-left k^2 (with size $k < 8$) out of 64 coefficients are computed while in triangle pattern only the coefficients within the area of right-angled triangle inside the previously mentioned square are computed. Therefore, the smaller the k value, the less processing time and energy consumption are required. The computed coefficients for both schemes are shown in Fig. 1 [35].

3.2.2. Fast zonal BinDCT based image compression

BinDCT (Binary Discrete Cosine Transformation) is fast integer friendly calculations of the DCT using the lifting scheme. BinDCT uses only sum and shift operations with integer numbers. Execution times and hardware requirements are reduced with no multiplication operations [36].

In BinDCT algorithm, image is divided into 8×8 blocks as in DCT algorithm. Lifting scheme based BinDCT is applied to all blocks of the

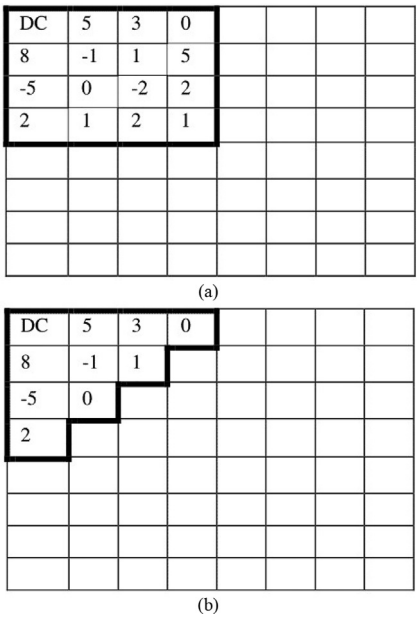

Fig. 1. 2-D 8-point DCT (k = 4) using (a) square pattern (b) triangle pattern.

image and 64 coefficients are computed. However, energy aware fast zonal BinDCT image compression method [13] computes only the significant zonal coefficients (top left square sub-matrix of size *k*×*k)* which are selected among the 64 DCT coefficients.

3.3. Energy harvesting systems

Energy harvesting is the process through which energy is acquired exploiting external ambient sources. The obtained energy is converted into electrical energy to provide additional energy for battery powered nodes. In this study, a piezoelectric (PZT) energy harvester which scavenges energy from vibration or strain, a Photo-Voltaic cell (PV) which scavenges energy from light and a Thermo-Electric Generator (TEG) which harvests electrical energy from temperature differences in indoor industrial environments are used.

3.3.1. Indoor solar energy harvesting system

One of the energy harvesting sources for industrial environment is artificial light. Photovoltaic cells are used to convert light energy into electrical energy. In this paper, an electrical circuit comprising a single diode and 15 PV cells presented in [37] are considered as the model of PV harvester.

The estimation of current from photovoltaic cells is critical for the estimation of harvested energy. The current–voltage (I–V) formula of the photovoltaic module according to four parameter model [38] is given by (8)

$$I_{PV} = I_L - I_0\left[exp\left(\frac{V_{PV} + I_{PV}R_s}{n_s V_t}\right) - 1\right]. \tag{8}$$

In (8), I_L represents the light generated current (*A*), I_0 denotes the reverse saturation current of the p-n diodes, R_s indicates the series resistance of the cells (Ω) and V_t is the thermal voltage of the cells. V_t symbolizes calculated using:

$$V_t = \frac{kT_c}{q}, \tag{9}$$

where k is the Boltzmann's constant, T_c is the cell temperature (*K*), and q is the charge of the electrons. The equation for power calculation for photovoltaic module is given as in (10)

$$P = IV. \tag{10}$$

The formula for determining maximum harvested power is obtained as follows [37]:

$$P_{PV}(V_{PV}) = V_{PV}I_{sc} - V_{PV}I_0\left[exp\left(\frac{V_{PV}}{n_s kT_c/q}\right)\right], \tag{11}$$

where the light generated current is approximately equal to the short circuit current ($I_L \approx I_{SC}$) and T_c is the ambient temperature. Harvested power calculations are performed using realistic environmental parameters and technical characteristics of the PV module.

3.3.2. Indoor thermal energy harvesting system

Another energy harvesting source for an industrial environment is thermal energy. A Thermo-Electric Generator (TEG) made of thermocouples which convert thermal energy into electrical energy. Electrical power is generated from temperature gradient exploiting Seeback's effect [39]. According to Seeback's effect, the open-circuit voltage, V_{oc} is given as:

$$V_{oc} = S * \Delta T = n * \alpha(T_H - T_C), \tag{12}$$

where, S represents the Seeback's coefficient of TEG and α represents the Seeback's coefficient of thermocouples. n is the number of thermocouples in TEG. T_H and T_C symbolize high temperature and low temperature, respectively. The electrical current that flows through the load resistance is obtained from (13)

$$I_{TEG} = \frac{V_{oc} - V_{TEG}}{R_{s,TEG}} = \frac{n * \alpha(T_H - T_C) - V_{TEG}}{R_{s,TEG}}. \tag{13}$$

In (13), $R_{s,TEG}$ denotes the internal electrical resistance of TEG. By using I-V characteristic of TEG, harvested power can be expressed as in (14):

$$P_{TEG}(V_{TEG}) = V_{TEG} * I_{TEG} = \frac{V_{TEG} * n * \alpha(T_H - T_C) - V_{TEG}^2}{R_{s,TEG}}. \tag{14}$$

3.3.3. Indoor vibration energy harvesting system

Ambient vibration can also be used as a source of harvesting power. Piezoelectricity is the preferred method to convert mechanical energy into electrical energy. The formula of generated power from vibration via a piezoelectric beam is described in (13) [40]

$$|P| = \frac{m\varsigma_e A^2}{4\omega\varsigma_T^2}, \tag{15}$$

where, m is the proof mass attached to piezoelectric cantilever beam, ω is the input frequency and A is the amplitude of acceleration in input vibration. ς_e is the electrical damping ratio and ς_T is the combined electrical and mechanical damping ratio ($\varsigma_T = \varsigma_e + \varsigma_m$).

3.4. Power management methods

A power management design aims to minimize energy consumption by controlling power usage, thus increasing the lifetime of the sensor node. The basic idea of the power management system is to shut down sensor node components when they are not needed.

In this study, a schedule-driven power management method is realized using MATSNL toolbox [10]. In this method, there are mainly two modes, namely low-power mode (sleep) and active (awake) mode in this model. For energy conservation, a sensor node is scheduled to be in sleep mode or awake mode according to its duty period and duty cycle. There are two timers used to trigger switching between low power and active mode when their durations end [10].

To compute a node's average power consumption and lifetime, the semi Markov chain model is used to form power state transitions shown in Fig. 2 [10]. In this model there are four stages, namely awake stage, sleep stage, process stage and communication stage. Since two kinds of scenario can occur in awake stage, this stage is divided into two virtual stages. The first one is the monitoring stage when an event is detected

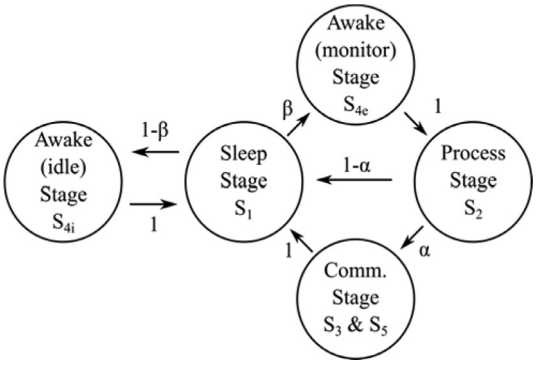

Fig. 2. State transition diagram.

Table 1
Schedule driven model.

Mode	Sensor	CPU	Radio
S_1	Off	Off	Off
S_2	Off	On	Off
S_3	Off	On	Tx
S_4	On	Idle	Off
S_5	Off	On	Rx

and the second one is the idle stage when no event is detected. The transitions among stages occur with certain probabilities. β is the probability of event detection while the sensor is in awake period. When an event is detected, the node proceeds to the processing stage, otherwise with 1-β probability it waits in the idle state until the awake period ends. After the node processes the event, with α probability the node shifts to the communication stage when there is an useful data to be sent. On the other hand, if there is no data to be sent, the sensor returns to sleep stage.

Sensor nodes have three main hardware units namely sensor, CPU, and radio. Each unit does not have to stay awake at every stage unless they are needed. For instance, radio is not necessary during the monitoring stage, hence the sensor turns the radio off to save energy. The five modes (S_1, S_2, S_3, S_4, and S_5) describe the status of sensor node's hardware units as shown in Table 1.

During the awake period, the sensor node senses the event, if there is no event detected, it waits in the idle stage until the awake period ends. The compression of images is performed in the processing stage. Finally, data transmission occurs in the communication stage.

To evaluate a sensor node's lifetime, the average power consumption per task is examined. Average power consumption and schedule driven sensor node lifetime can be determined by (16) and (17)

$$P_{sch}(\beta) = \frac{P_e + \frac{\beta}{T_c} M_E}{1 + \frac{\beta}{T_c} M_T}, \tag{16}$$

$$T_L(\beta) = \frac{(1 + \frac{\beta}{T_c} M_T) E_{total}}{P_e + \frac{\beta}{T_c} M_E}. \tag{17}$$

In (14) and (15), P_e represents the average power consumption without event detection. M_E and M_T are the average residual energy and the average residual time spent in case of an event detection, respectively. T_c represents the duty period duration. E_{total} is the total available energy. The average residual energy (M_E) spent when the node is awake and detects an event can be formulated as (18) [8]:

$$M_E = T_{S2} * P_{S2} + \alpha * (T_{S3} * P_{S3} + C_R) - \frac{T_W * (T_W + 2 * T_E)}{2 * (T_W + T_E)} * P_{S4}. \tag{18}$$

Table 2
Simulation parameters for log normal shadowing channel model.

Parameters	Unit	Value
Path loss at distance d_0,$PL(d_0)$	dB	63.57
Reference distance, d_0	m	0.5
Path loss exponent, n	–	2.40
Shadowing standard deviation, σ	dB	4.79
Noise floor, P_n	dBm	−93.0
Output power, P_t	dB	0
Frame size, f	bytes	128
Preamble length, l	bytes	12

The average residual time (M_T) is formulated as:

$$M_T = T_{S2} + \alpha * T_{S3} - \frac{T_W * (T_W + 2 * T_E)}{2 * (T_W + T_E)}. \tag{19}$$

The power consumed when no events are detected is calculated as:

$$P_e = P_{S1} + d * (P_{S4} - P_{S1}) + \frac{C_P}{T_c}. \tag{20}$$

In (17), (18), and (19), T_{S2} and T_{S3} represent the average processing and transmission time per event, respectively. T_W is the CPU awake duration and T_E is the event duration. P_{S1}, P_{S2}, P_{S3} and P_{S4} are the power consumed in idle state, processing state, communication state, and monitoring state, respectively. C_P is the CPU wake-up energy cost and C_R is the radio wake-up energy cost, α is the probability of the sensor node switching from processing stage to communication stage and d is duty period.

Finally, lifetime improvement is calculated using (21):

$$Lifetime\_improvement = \frac{Lifetime_{with\_CompAndEH} - Lifetime_{un\,mod\,ified}}{Lifetime_{un\,mod\,ified}} * 100. \tag{21}$$

4. Performance results

In this paper, the sensor node lifetime transmitting image data in an industrial environment is examined. Log normal shadowing is the preferred channel model. Industrial environment field trial based parameters presented in Table 2 are used in the channel model [41]. The simulations are performed with schedule-driven Telos and Mica2 sensor motes [42].

In this study, the Carrier Sense Multiple Access (CSMA) MAC protocol is used as the channel access scheme. In CSMA, the radio senses the channel to control whether it is busy or not before transmitting data. Moreover, if a packet is not successfully transmitted due to channel conditions, node attempts to retransmit the packet. The number of retransmissions is determined according to PRR. The maximum number of retransmissions is set to three to prevent extreme lifetime degradation of the sensor node. PRR value for different distance values are shown in Fig. 3. As shown, PRR significantly decreases over distance. Although log-normal shadowing is a probabilistic model, mean value of PRR is used in simulation experiments.

To decrease the image data size, the Fast-Zonal DCT and Fast-Zonal BinDCT compression methods described in Section 3 are used. In simulation experiments, square-based methods with different k parameters are utilized since they are proven to be superior to triangle based approaches in terms of energy distortion tradeoff [35]. The execution time for compressing a 256×256 sized image encoded at 0.5 bpp (bit per pixel) with different methods are evaluated according to processing time for compressing 8×8 DCT block on Telos and Mica2 motes [35,13,43] and shown in Table 3. The extra time compressing image data takes is added to the duration of processing state (S_2). All the results are shown from Figs. 4 to 11.

Firstly, the figures show that using any of the mentioned compression approaches generally improves lifetime under the simulated conditions compared to the case without compression. This is mainly due

Table 3
Execution time for compressing 256 × 256 image.

	DCT based with k = 8 (S-8)	DCT based with k = 4 (S-4)	DCT based with k = 2 (S-2)	BinDCT based with k = 8 (P-8)	BinDCT based with k = 4 (P-4)	BinDCT based with k = 2 (P-2)
Telos Time (ms)	44,851	38,502	27,136	4018	2684	1428
Mica2 Time (ms)	19,760	11,124	6288	1188	686	339

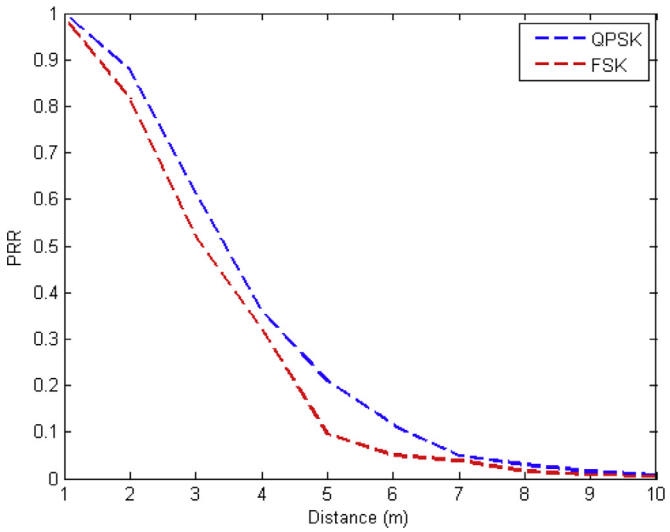

Fig. 3. Distance and PRR relation with different modulation schemes.

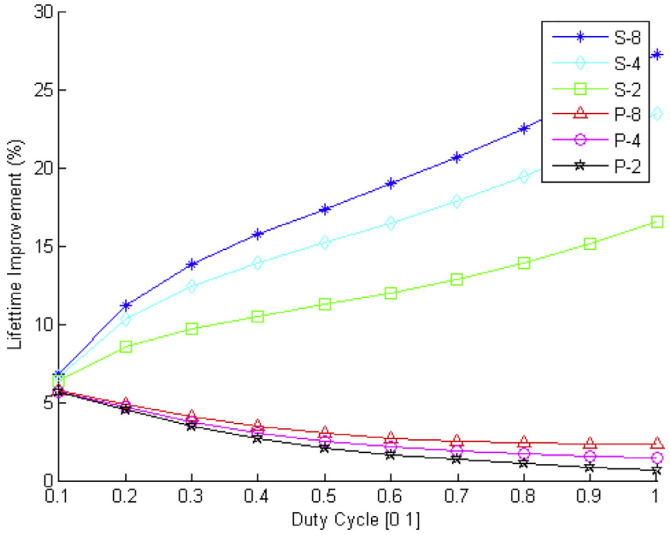

Fig. 4. Lifetime improvement with different image compression approaches at 10 m distance for Telos.

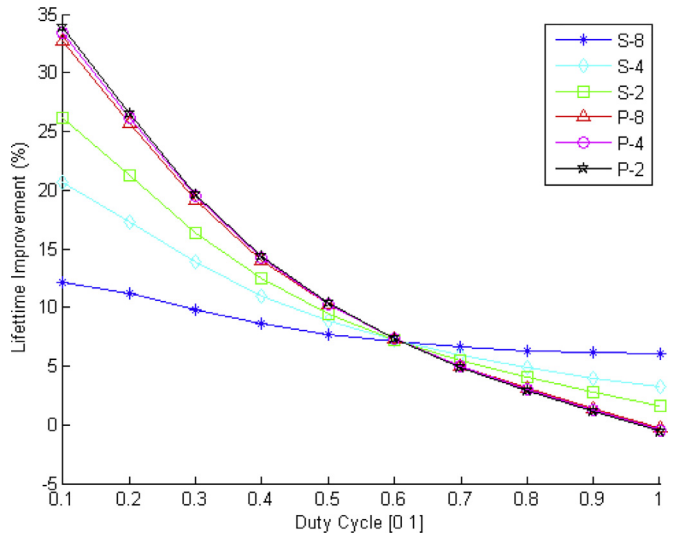

Fig. 5. Lifetime improvement with different image compression approaches at 10 m distance for Mica2.

to extended processing stage (S_2) duration where compression occurs. The power requirement of S_2 state is lower than that of other states due to having only CPU in active status. Therefore, extended duration of S_2 state causes average power consumption to decrease within a single cycle depicted in Fig. 2.

In Figs. 4 and 5, lifetime improvement different compression approaches provide at varying duty cycle values for Telos and Mica2 motes and 10 m of transmission distance are depicted. In the figures, lifetime improvement trend is decided by mainly additional processing duration and the power requirement for processing. If the additional time is long enough and the processing power is low enough, the average power consumption will decrease, which increases the lifetime. For Telos mote, DCT compression provides higher lifetime improvement for all duty cycle values. However, while the impact of DCT compression on lifetime is increased over the horizontal axis, the impact of BinDCT is decreased. The longer duration of DCT based compression combined with very low processing power requirements of Telos mote causes the decrease on the average power consumption with compression to be higher as duty cycle increases. This is not the case for any other combination of mote and compression types since either the execution time is short or processing power requirement is relatively high for S_2 state. Therefore, BinDCT compression methods for Telos mote and all compression methods for Mica2 mote provide decreased lifetime improvement over the horizontal axis.

For Mica2, the impact of DCT based compressions (S-8, S-4, S-2) are less than BinDCT based compressions (P-8, P-4, P-2) until duty cycle of 0.6 despite their longest execution durations. This is because the average power consumption of Mica2 without compression is smaller than the power consumption of S_2 state. Beyond 0.6 duty cycle the average power consumption without compression is increased above the power consumption of S_2 state. In this region, the longer the compression method takes the more the average power consumption is decreased, providing bigger lifetime improvement.

Similar to Figs. 4 and 5, Figs. 6 and 7 shows lifetime improvement for different transmission distances for Telos and Mica2 motes with 0.1 duty cycle. In the figures, the impact of compression gets more explicit at higher distance values. Without compression, large data sizes and long transmission distances require extremely high energy levels for transmission. However, reducing data size via compression decreases required energy amounts tremendously. Therefore, at longer distances where the energy requirement per bit transmission is higher, the impact of data size reduction is more explicit. The negative impact on lifetime when Mica2 mote is used at transmission distances lower than 5 m is the result of not having significantly low power consumption for processing compared to transmission. At shorter distances, the energy spent for packet transmission is lower due to less number of retransmissions. Therefore, the additional energy spent for extended S_2 state is too high

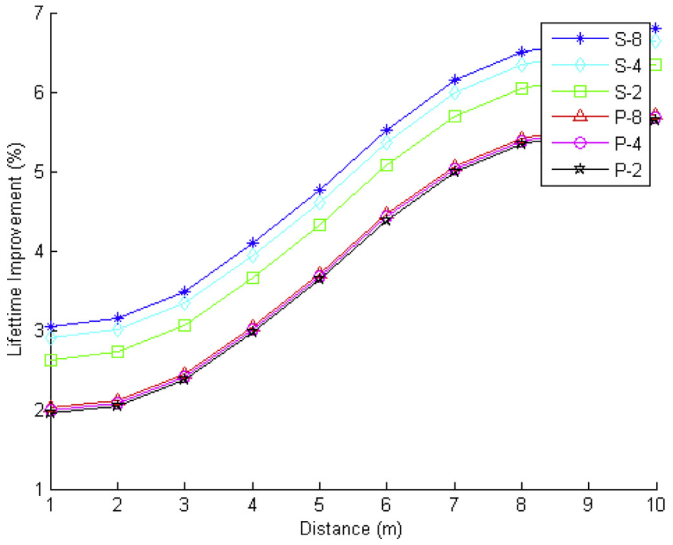

Fig. 6. Lifetime improvement with different image compression approaches at 0.1 duty cycle for Telos.

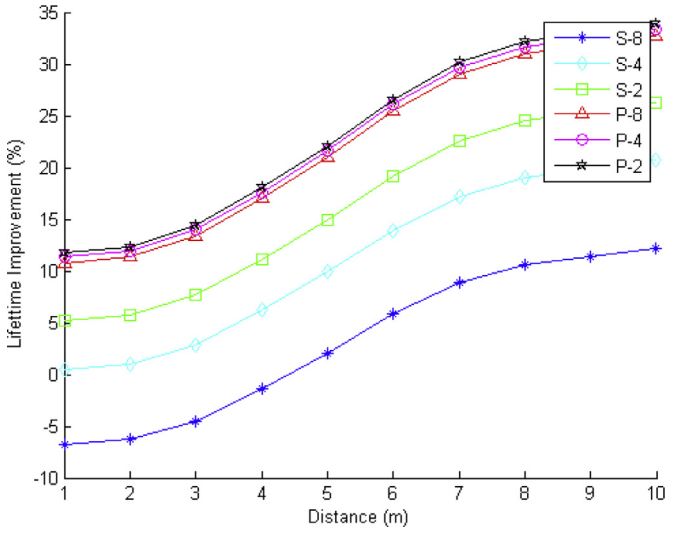

Fig. 7. Lifetime improvement with different image compression approaches at 0.1 duty cycle for Mica2.

to be compensated by the decreased transmission energy due to size reduction, decreasing the lifetime.

In Figs. 6 and 7, the compression method that creates the biggest impact is different. While DCT methods provide higher improvements for Telos mote, it is BinDCT methods for Mica2 mote. As stated before, the figures use 0.1 duty cycle and at this value the average power consumption of Mica2 without compression is lower than that of S_2 state. Therefore, longer compression methods increase average power consumption closer to the power consumption of S_2 state, providing less lifetime improvement.

Figs. 8 and 9 present lifetime improvement at different duty cycles when compression and harvesting methods are combined together for Telos and Mica2 motes. Although longer execution times cause bigger lifetime improvement when average power consumption without compression is bigger than power consumption of S_2 state, it causes degradation in the number of cycles performed throughout the lifetime, hence the measurements. Consequently, BinDCT (P-2) is the preferred compression method in Figs. 8–11 since it provides lifetime improvement without decreasing the number of measurements (cycles) substantially throughout the node's lifetime. Moreover, the parameters that are used

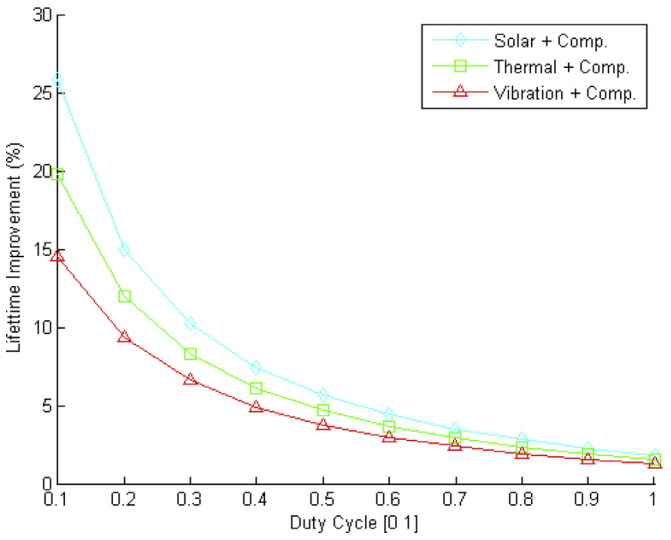

Fig. 8. Lifetime improvement with image compression (P-2) and different energy harvesting methods at 10 m distance for Telos.

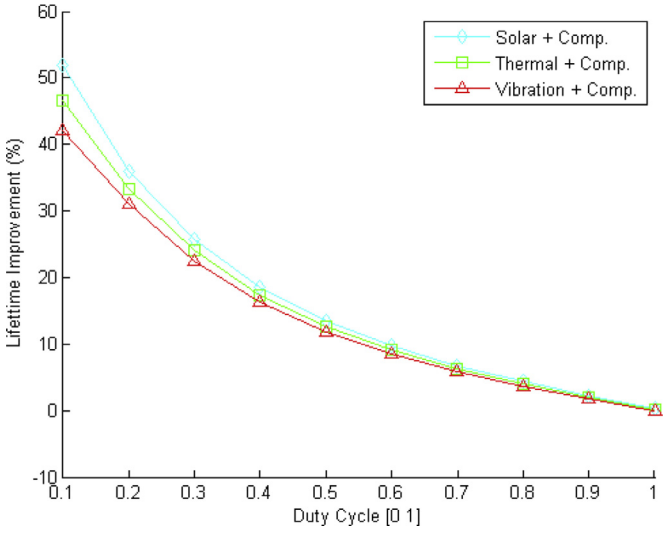

Fig. 9. Lifetime improvement with image compression (P-2) and different energy harvesting methods at 10 m distance for Mica2.

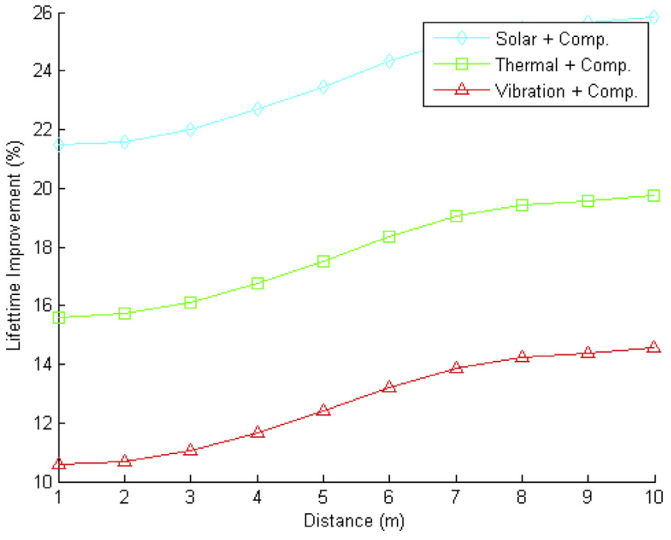

Fig. 10. Lifetime improvement with image compression (P-2) and different energy harvesting methods at 0.1 duty cycle for Telos.

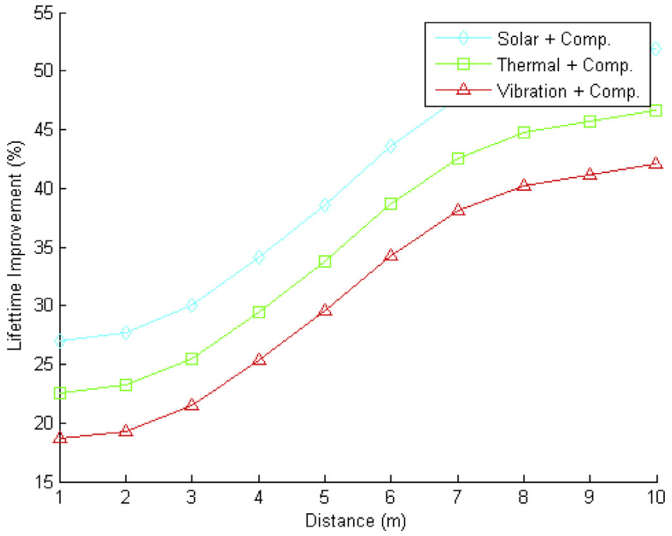

Fig. 11. Lifetime improvement with image compression (P-2) and different energy harvesting methods at 0.1 duty cycle for Mica2.

Table 4
Simulation parameters for indoor solar harvester.

Parameters	Unit	Value
Ambient temperature, T_c	K	295
Number of PV cells, n	–	15
Current of p-n nodes, I_0	A	1×10^{-9}
Current of light irradiance, I_{sc}	μA	150
Charge of electron, q	C	1.6022×10^{-19}
Boltzmanns constant, k	JK^{-1}	1.3807×10^{-23}

Table 5
Simulation parameters for thermal harvester.

Parameters	Unit	Value
Temperature differences, ΔT	K	10
Number of thermocouples, n	–	5200
Seeback's coefficient, α	mV/K	0.21
Internal electrical resistance, R_S	kΩ	82

Table 6
Simulation parameters for vibration harvester.

Parameters	Unit	Value
Frequency	Hz	71
Voltage	V	4.8
Current	Ma	0.05

Table 7
Average harvested power.

Harvester	Unit	Value
Solar	mW	0.4947
Thermal	mW	0.3635
Vibration	mW	0.2400

in energy harvesting methods are provided in Tables 4–6. Considering the conditions of an industrial environment, evaluations have been performed with 1010 lx lighting conditions and 3.6 V output voltage of solar panel for indoor solar harvester. The performance of the thermal energy harvester is simulated with 10 K temperature difference and 5.5 V output voltage. The average amount of harvestable power from indoor solar, thermal and vibration harvesters are calculated according to formulas presented in Section 3 and listed in Table 7. Among these harvesters, the indoor solar system harvests the maximum power which is 0.4947 mW.

In Fig. 8 the impact of energy harvesting on node lifetime is explicit compared to Fig. 4, where the impacts of different compression methods are depicted. The lifetime improvement that was between 5.6% and 0.7% is now increased to between 14.5% and 1.2% using vibration harvester. The impacts are even higher using thermal and solar harvesters. For Mica2 mote, Fig. 9 shows that the lifetime improvement is increased to between 42.1% and −0.1% which was between 33.9% and −0.6% before harvesting.

Figs. 10 and 11 show lifetime improvement values when harvesting is integrated at different transmission distances. For Telos, the lifetime improvement without harvesting was between 2% and 5.6% as shown in Fig. 6. Using vibration harvester, the improvement is increased to the range between 10.6% and 14.6%. Similarly, the range for Mica2 mote which was lying between 11.8% and 33.9% was improved to between 18.7% and 42.1%. Considering these results, network parameters, such as duty cycle and distance values, should be arranged according to applications needs.

5. Conclusion

In this paper, the lifetime of a sensor node that transmits image with and without compression has been analyzed in an industrial environment. The analysis has been conducted using a log-normal shadowing model as the channel model and a schedule-driven algorithm as power management scheme. In addition, the impact of three different harvesting systems, namely indoor solar harvester, thermal harvester and vibration-based harvester are examined utilizing different compression methods with Telos and Mica2 sensor motes.

Performance results show that the energy spent for extra processing operations during compression is smaller than the difference between the communication energy requirements of the original and compressed images. Therefore, it is shown that node lifetime is improved especially at longer transmission distances when compression is employed. Moreover, our analysis shows that energy harvesting techniques extend the node lifetime significantly. For example, by using BinDCT compression methods and solar harvesting, the maximum improvement for Mica2 is 51.8% whereas the maximum improvement for Telos is 25.8%. As a result, compression and energy harvesting methods are viable solutions to the lifetime problem of sensor nodes when used with proper power management methods tailored to application requirements. Future work includes the development of energy harvesting based communication solutions for different industrial applications, sensor motes and compression schemes.

Acknowledgment

The work of V.C. Gungor was supported by BAGEP and AGU Foundation.

References

[1] J.P.J. Peixoto, D.G. Costa, Wireless visual sensor networks for smart city applications: A relevance-based approach for multiple sinks mobility, Futur. Gener. Comput. Syst. 76 (November) (2017) 51–62.
[2] I.F. Akyildiz, T. Melodia, K.R. Chowdhury, Wireless multimedia sensor networks: applications and testbeds, Proc. IEEE 96 (10) (2008) 1588–1605.
[3] T. AlSkaif, B. Bellalta, M.G. Zapata, J.M. Barcelo Ordinas, Energy efficiency of MAC protocols in low data rate wireless multimedia sensor networks: a comparative study, Ad Hoc Networks 56 (March) (2017) 141–157.
[4] K.S. Low, W.N.N. Win, M.J. Er, Wireless sensor networks for industrial environments, in: Proceedings of International Conference on Comput. Intell. Model. Control Autom. Int. Conf. Intell. Agents, Web Technol. Internet Commer., 2, 2005, pp. 271–276.
[5] V.C. Gungor, G.P. Hancke, Industrial wireless sensor networks: challenges, design principles, and technical approaches, IEEE Trans. Ind. Electron. 56 (10) (2009) 4258–4265.
[6] I.F. Akyildiz, T. Melodia, K.R. Chowdhury, A survey on wireless multimedia sensor networks, Comput. Networks 51 (4) (2007) 921–960.
[7] M. Erol-Kantarci, H.T. Mouftah, Wireless multimedia sensor and actor networks for the next generation power grid, Ad Hoc Networks 9 (4) (2011) 542–551.
[8] J. Yick, B. Mukherjee, D. Ghosal, Wireless sensor network survey, Comput. Networks 52 (12) (2008) 2292–2330.

[9] H. Yetgin, K.T.K. Cheung, M. El-Hajjar, L. Hanzo, A survey of network lifetime maximization techniques in wireless sensor networks, Proc. IEEE Commun. Surv. Tut. 19 (2) (2017) 828–854.
[10] D. Jung, T. Teixeira, A. Savvides, Sensor node lifetime analysis: models and tools, ACM Trans. Sen. Netw. 5 (1) (2009) 1–33.
[11] A. Willig, Recent and emerging topics in wireless industrial communications: a selection, IEEE Trans. Ind. Informatics 4 (2) (2008) 102–124.
[12] A. Newell, K. Akkaya, Distributed collaborative camera actuation for redundant data elimination in wireless multimedia sensor networks, Ad Hoc Networks 9 (4) (2011) 514–527.
[13] Y.A. Phamila, R. Amutha, Low-complex energy-aware image communication in visual sensor networks, J. Electron. Imaging 22 (4) (2013) 41107–41113.
[14] F.K. Shaikh, S. Zeadally, Energy harvesting in wireless sensor networks: a comprehensive review, Renew. Sustain. Energy Rev. 55 (March) (2016) 1041–1054.
[15] M. Nasri, A. Helali, H. Sghaier, H. Maaref, Adaptive image transfer for wireless sensor networks (WSNs), in: Proceedings of 5th International Conference on Design and Technology of Integrated Systems in Nanoscale Era, March, 2010, pp. 1–7.
[16] P.N. Huu, V. Tran-Quang, T. Miyoshi, Energy threshold adaptation algorithms on image compression to prolong WSN lifetime, in: Proceedings of International Symposium on Wireless Communication Systems, September, 2010, pp. 834–838.
[17] E. Sun, X. Shen, H. Chen, A low energy image compression and transmission in wireless multimedia sensor networks, Procedia Eng 15 (2011) 3604–3610.
[18] W. Li, Z.P. Pang, Z.J. Liu, SPIHT algorithm combined with huffman encoding, in: Proceedings of International Symposium on Intelligent Information Technology and Security Informatics, April, 2010, pp. 341–343.
[19] Z. Wei, S. Lijuan, G. Jian, L. Linfeng, Image compression scheme based on PCA for wireless multimedia sensor networks, J. China Univ. Posts Telecommun. 23 (1) (2016) 22–30.
[20] R. Hemalatha, S. Radha, S. Sudharsan, Energy-efficient image transmission in wireless multimedia sensor networks using block-based compressive sensing, in: Proceedings of Computers & Electrical Engineering, May, 44, 2015, pp. 67–79.
[21] G. Nikolakopoulos, P. Stavrou, D. Tsitsipis, D. Kandris, A. Tzes, T. Theocharis, A dual scheme for compression and restoration of sequentially transmitted images over wireless sensor networks, Ad Hoc Networks 11 (1) (2013) 410–426.
[22] N.R. Kidwai, E. Khan, M. Reisslein, ZM-SPECK: a fast and memoryless image coder for multimedia sensor networks, IEEE Sens. J. 16 (8) (2016) 2575–2587.
[23] O. Orhan, D. Gunduz, E. Erkip, Source-channel coding under energy, delay, and buffer constraints, IEEE Trans. Wirel. Commun. 14 (7) (2015) 3836–3849.
[24] M. Calvo-Fullana, J. Matamoros, C. Anton-Haro, Reconstruction of correlated sources with energy harvesting constraints in delay-constrained and delay-tolerant communication scenarios, IEEE Trans. Wirel. Commun. 16 (3) (2017) 1974–1986.
[25] R. Shigeta, et al., Ambient-RF-energy-harvesting sensor node with capacitor-leakage-aware duty cycle control, in: Proceedings of IEEE Sensors, October, 2012, pp. 1–4.
[26] A. Hande, T. Polk, W. Walker, D. Bhatia, Indoor solar energy harvesting for sensor network router nodes, Microprocess. Microsyst. 31 (6) (2007) 420–432.
[27] A. Elefsiniotis, N. Kokorakis, T. Becker, U. Schmid, Performance of a low temperature energy harvesting device for powering wireless sensor nodes in aircrafts applications, in: Proceedings of Transducers Eurosensors International Conference on Solid-State Sensors, Actuators Microsystems, 2013, pp. 2276–2279.
[28] M. Karimi, A.H. Karimi, R. Tikani, S. Ziaei-Rad, Experimental and theoretical investigations on piezoelectric-based energy harvesting from bridge vibrations under travelling vehicles, Int. J. Mech. Sci. 119 (July) (2016) 1–11.
[29] J. Sankman, D. Ma, A 12-μW to 1.1-mW AIM piezoelectric energy harvester for time-varying vibrations with 450-nA IQ, IEEE Trans. Power Electron. 30 (2) (2015) 632–643.
[30] M. Zuniga, B. Krishnamachari, Analyzing the transitional region in low power wireless links, in: Proceedings of IEEE Communications Society Conference on Sensor Ad Hoc Communications Networks, 2004, pp. 517–526.
[31] C. Eris, M. Saimler, V.C. Gungor, E. Fadel, I.F. Akyildiz, Lifetime analysis of wireless sensor nodes in different smart grid environments, Wireless Networks 20 (7) (2014) 2053–2062.
[32] M.C. Vuran, I.F. Akyildiz, Error control in wireless sensor networks: a cross layer analysis, IEEE/ACM Trans. Netw. 17 (4) (2009) 1186–1199.
[33] S. Chen, J. Liu, M. Wu, Z. Sun, DCT-based adaptive data compression in wireless sensor networks, in: Proceedings of International Conference Computer Communications and Networks, August, 2016, pp. 1–5.
[34] A.S. Dhavale, G.B. Gadekar, M.S. Bhagat, V.B. Jagtap, Discrete cosine transform based image compression, Int. J. Adv. Comput. Electron. Technol. 3 (1) (2016) 45–52.
[35] L. Makkaoui, V. Lecuire, J.-M. Moureaux, Fast zonal DCT-based image compression for wireless camera sensor networks, in: Proceedings of International Conference on Image Processing Theory, Tools Applications, July, 2010, pp. 126–129.
[36] A. Ben Abdelali, I. Chatti, M. Hannachi, A. Mtibaa, Efficient BinDCT hardware architecture exploration and implementation on FPGA, J. Adv. Res. 7 (6) (2016) 909–922.
[37] Y.K. Tan, S.K. Panda, Energy harvesting from hybrid indoor ambient light and thermal energy sources for enhanced performance of wireless sensor nodes, IEEE Trans. Ind. Electron. 58 (9) (2011) 4424–4435.
[38] A.N. Celik, N. Acikgoz, Modelling and experimental verification of the operating current of mono-crystalline photovoltaic modules using four- and five-parameter models, Appl. Energy 84 (1) (2007) 1–15.
[39] K. Uchida, et al., Observation of the spin Seebeck effect, Nature 455 (7214) (2008) 778–781.
[40] Y. Yoon, W. Park, K.H.H. Li, Y.Q. Ng, Y. Song, A study of piezoelectric harvesters for low-level vibrations in wireless sensor networks, Int. J. Precis. Eng. Manuf. 14 (7) (2013) 1257–1262.
[41] G. Gao, H. Zhang, L. Li, Performance evaluation of WSNs-based link quality estimation metrics for industrial environments, in: Proceedings of Advances Technologies Ad Hoc Sensor Networks, 2014, pp. 69–79.
[42] J. Polastre, R. Szewczyk, D. Culler, Telos: enabling ultra-low power wireless research, in: Proceedings of the 4th International Symposium on Information Processing in Sensor Networks, 2005.
[43] J.-M. Moureaux, Fast zonal DCT for energy conservation in wireless image sensor networks, Electron. Lett. 48 (2) (2012) 125–127.